Biochimica et Biophysica Acta 1818 (2012) 617–626

Contents lists available at SciVerse ScienceDirect

Biochimica et Biophysica Acta

journal homepage: www.elsevier.com/locate/bbamem

NMR structure and dynamics of a designed water-soluble transmembrane domain of nicotinic acetylcholine receptor

Tanxing Cui [a,b], David Mowrey [a,c], Vasyl Bondarenko [a], Tommy Tillman [a], Dejian Ma [a], Elizabeth Landrum [b], Jose Manuel Perez-Aguilar [d], Jing He [d], Wei Wang [d], Jeffery G. Saven [d], Roderic G. Eckenhoff [e], Pei Tang [a,c,f], Yan Xu [a,b,f,*]

[a] Department of Anesthesiology, University of Pittsburgh School of Medicine, USA
[b] Department of Structural Biology, University of Pittsburgh School of Medicine, USA
[c] Department of Computational Biology, University of Pittsburgh School of Medicine, USA
[d] Department of Chemistry, University of Pennsylvania, USA
[e] Department of Anesthesiology and Critical Care Medicine, University of Pennsylvania Perelman School of Medicine, USA
[f] Department of Pharmacology & Chemical Biology, University of Pittsburgh School of Medicine, USA

ARTICLE INFO

Article history:
Received 16 October 2011
Accepted 22 November 2011
Available online 3 December 2011

Keywords:
Nicotinic acetylcholine receptor
Water-solubilization
Nuclear magnetic resonance (NMR) spectroscopy
Membrane protein
Computational protein redesign

ABSTRACT

The nicotinic acetylcholine receptor (nAChR) is an important therapeutic target for a wide range of pathophysiological conditions, for which rational drug designs often require receptor structures at atomic resolution. Recent proof-of-concept studies demonstrated a water-solubilization approach to structure determination of membrane proteins by NMR (Slovic et al., PNAS, 101: 1828–1833, 2004; Ma et al., PNAS, 105: 16537–42, 2008). We report here the computational design and experimental characterization of WSA, a water-soluble protein with ~83% sequence identity to the transmembrane (TM) domain of the nAChR α1 subunit. Although the design was based on a low-resolution structural template, the resulting high-resolution NMR structure agrees remarkably well with the recent crystal structure of the TM domains of the bacterial *Gloeobacter violaceus* pentameric ligand-gated ion channel (GLIC), demonstrating the robustness and general applicability of the approach. NMR T_2 dispersion measurements showed that the TM2 domain of the designed protein was dynamic, undergoing conformational exchange on the NMR timescale. Photoaffinity labeling with isoflurane and propofol photolabels identified a common binding site in the immediate proximity of the anesthetic binding site found in the crystal structure of the anesthetic-GLIC complex. Our results illustrate the usefulness of high-resolution NMR analyses of water-solubilized channel proteins for the discovery of potential drug binding sites.

1. Introduction

Nicotinic acetylcholine receptors (AChRs) belong to a superfamily of neurotransmitter-gated ion channels, which also include glycine (Gly), γ-amino-butyric acid type A ($GABA_A$), and serotonin ($5\text{-}HT_3$) receptors. These receptors, composed of five homologous subunits in a pentameric assembly, mediate fast synaptic transmissions. All subunits are comprised of a large extracellular domain, four transmembrane (TM) domains, and a long intracellular loop linking the third and fourth TM domains [1,2]. Mutagenesis and functional investigations have shown that the binding of at least two agonists at the interfaces of the extracellular domains triggers the channel opening, allowing ions to pass through a TM pore surrounded by the TM2 helices from the five subunits.

The most studied member of this receptor superfamily is the highly abundant nAChR found in the *Torpedo* electric organs. The *Torpedo* nAChR, consisting of two α1 subunits and one each of β1, γ, and δ subunits, is homologous to the mammalian muscle-type nAChR responsible for rapid signaling at the neuromuscular junction. Although no atomic resolution structure is yet available for nAChRs, a 4-Å-resolution structure model has been determined by pioneering cryo-electron microscopy (cryo-EM) work on the *Torpedo* nAChR [3,4]. More recently, high-resolution structural insights were gained from several crystal or NMR structures of related proteins, including an isolated extracellular domain of the nAChR α1 subunit bound to α-bungarotoxin [5], isolated four TM domains of the nAChR β2 subunit [6], the snail acetylcholine binding protein [7] which resembles the extracellular domain of the nAChR, and two prokaryotic pentameric ligand-gated ion channels from the bacterium *Erwinia chrysanthemi* (ELIC) [8] and the cyanobacterium *Gloeobacter violaceus* (GLIC) [9,10]. The overall architecture of the extracellular domains is similar among the currently available structures. The TM domains, however, exhibit significant variation in high-resolution detail. The discrepancy among

* Corresponding author at: 2048 Biomedical Science Tower 3, University of Pittsburgh School of Medicine, 3501 Fifth Avenue, Pittsburgh, PA 15260, USA. Tel.: +1 412 648 9922; fax: +1 412 648 8998.
E-mail address: xuy@anes.upmc.edu (Y. Xu).

0005-2736/$ – see front matter © 2011 Elsevier B.V. All rights reserved.
doi:10.1016/j.bbamem.2011.11.021

the TM domain structures may result from the difference in the membrane mimetic environments used for the structure determination, or from the difference in the ion-conducting states of the TM segments. It is worth noting that the 4-Å-resolution cryo-EM structure of the muscle-type nAChR shows four straight long helices in the TM domains. In contrast, the GLIC and ELIC crystal structures and the nAChR β2 NMR structure all exhibit relatively short and curved helical structures. The cryo-EM nAChR structure is presumably in the closed-channel state, whereas GLIC is either in a desensitized state or in a non-physiological artificial state due to the unexpected presence of detergent molecules within the aqueous pore. The ELIC crystal structure is thought to be in a collapsed state. Potential interactions with cholesterol, which are present in the eukaryotic membrane but absent in the prokaryotic membrane, can add another layer of complexity in TM domain structure determination.

The uncertainty in the TM domain structures reflects the technical difficulties associated with the structure determination of TM channel proteins. Crystallization trials involve the use of nonnative detergents that may or may not support the functional fold of the TM domains. The success in the expression, purification, and crystallization of prokaryotic channels such as ELIC and GLIC does not readily translate into practice for mammalian channels, which are difficult to overexpress in suitable quantities for structural studies. Because of their large hydrophobic surface in the TM segments, and the need for post-translational modifications, mammalian channel proteins are also prone to aggregation, rendering standard solution-phase purification methods ineffective. Most biophysical studies involve dispersing membrane proteins in aqueous media, usually using detergents, lipids, auxiliary proteins, and other membrane-mimetic mixtures. Obtaining conditions to achieve monodispersity for X-ray crystallography or NMR studies remains a sensitive and exceedingly time consuming process.

An alternate, systematic approach is to redesign membrane proteins to remove the exposed hydrophobic exterior. In essence, TM proteins are transformed into soluble ones while retaining important structural and functional features. Using computational approaches, water-soluble variants of integral membrane proteins have been designed to facilitate structural studies. Recently, a computationally designed water-soluble variant of the bacterial potassium ion channel KcsA has been accomplished [11,12] and its high-resolution structure has been elucidated by NMR [13]. The NMR structure of one of the three designed sequences of water-solubilized KcsA (WSK3) is in striking agreement with the crystal structure of the wild-type protein [13,14]. These findings emphasize the promise of developing water-soluble variants of membrane proteins suitable for biophysical studies and potentially for structure-based drug discovery.

In this study, we present a similar approach for the TM domains of the nAChR α1 subunit. A water-soluble variant of the TM domains was computationally designed, resulting in the replacement of 23 hydrophobic residues with hydrophilic ones at the lipid-exposed surface. The resulting protein, called water-soluble acetylcholine receptor channel (WSA), was experimentally expressed and purified, and its structures determined using high-resolution NMR. Because the nAChRs are potential molecular targets for general anesthetics [15–19], we also determined the binding of two representative anesthetics, azi-isoflurane and azi-propofol, to the designed protein using photoaffinity labeling. We found that the designed protein retained an overall four-helix bundle topology and overlapped remarkably well with the crystal structure of the GLIC TM domains. A common binding site was identified for azi-isoflurane and azi-propofol in the general vicinity of a propofol binding site found in the crystal structure of anesthetic-bound GLIC. These results provide additional experimental evidence for the general applicability of the water solubilization approach to high-resolution structural investigation of membrane proteins.

2. Methods

2.1. Computational sequence design for water solubilization

The design principle involves the identification and redesign of exposed hydrophobic residues in the TM domains in order to transform a membrane protein into a completely or partially soluble protein while maintaining the structure- and function-related properties. The redesign of the nAChR α1 subunit was based on the 4-Å-resolution cryo-EM structure model as a template (PDB accession code: 1OED; Fig. 1a) [3,4]. The exposed residues were selected as those with more than 40% solvent exposure (Fig. 1b) according to GETAREA1.1 [20]. Residues targeted for mutation were both hydrophobic (AFILMVW) and expected to reside in the TM region [3]. Hydrophobic residues at the interfaces between helices within the subunit were retained as in the wild type protein.

The site-specific probabilities of the amino acids at the potential mutation sites were calculated as described previously [11,21–25]. For each of the sites, all 20 amino acids were permitted while the remaining residues were constrained as wild type. Side chain conformations were restricted to those from a library of frequently observed conformations (rotamer states) [26] with at most 10 rotamer states per amino acid. Two energy functions, averaged over the sequence of the entire protein, were constrained to characterize the ensemble of soluble variants. The first energy term accounts for the interatomic interactions using a molecular mechanics force field (the AMBER force field) [27]. The second term quantifies the hydrophobic potential (environmental or solvation energy) that was constrained to an averaged value expected for a soluble protein with a size similar to the TM domains of the nAChR α1 subunit [11].

The computation for site-specific probabilities of amino acids at each mutation position was carried out in two stages. The first stage used the most probable amino acids at each of the targeted positions. At the second stage, only the sites where one amino acid was highly favored (probability of an amino acid exceeding 0.8) were constrained to that most probable amino acid. At the rest of the positions, an additional constraint was imposed to increase the diversity of different amino acids that appear in the final sequence. Amino acid diversity is desirable to avoid spectral over-crowding in the NMR spectra, thereby facilitating spectral assignment and structure determination. The sequence diversity constraint was implemented as an inverse participation ratio:

$$\frac{1}{m_{eff}} = \sum_{\alpha=1}^{m} f^2(\alpha) \tag{1}$$

$$f(\alpha) = \frac{1}{\nu}\sum_{i=1}^{\nu} \omega_i(\alpha) \tag{2}$$

where m is the number of possible amino acids, e.g., $m = 20$ if all the naturally occurring amino acids are permitted. The function $f(\alpha)$ is the frequency with which amino acid α appears among the sequences and is

Fig. 1. Sequence redesign. (a) Ribbon representation of the pentameric structural template (PDB code: 2BG9) of nicotinic acetylcholine receptor (nAChR) used for the water solubilization sequence redesign. (b) The transmembrane domain of the α1 subunit in van der Waals representation before (left) and after (right) the computational redesign. Residues are colored by amino acid types: Green: hydrophilic (GNQSTY); white: hydrophobic (ACFILMPVW); blue: basic (HKR); and red: acidic (DE). (c) Cartoon representation of helix configuration in water-solubilized acetylcholine receptor (WSA). A polyglycine linker was added between TM1 (helical N-terminus) and TM4 (helical C-terminus) so that the TM domains can be expressed as a single chain. (d) Sequences of the transmembrane domains of nAChR α1 subunit, two calculated water-solubilization designs, and the bacterial pentameric ion channel GLIC are aligned for comparison. Water-solubilization mutations are marked in red. The most probable mutations are in italic boldface. Mutations changed by the inclusion of sequence diversity constraints are highlighted in green. Putative pore-lining residue positions are highlighted in blue. The transmembrane domain helices in the corresponding structures are underlined for comparison. Conformation heterogeneity in WSA is underlined with dashed lines.

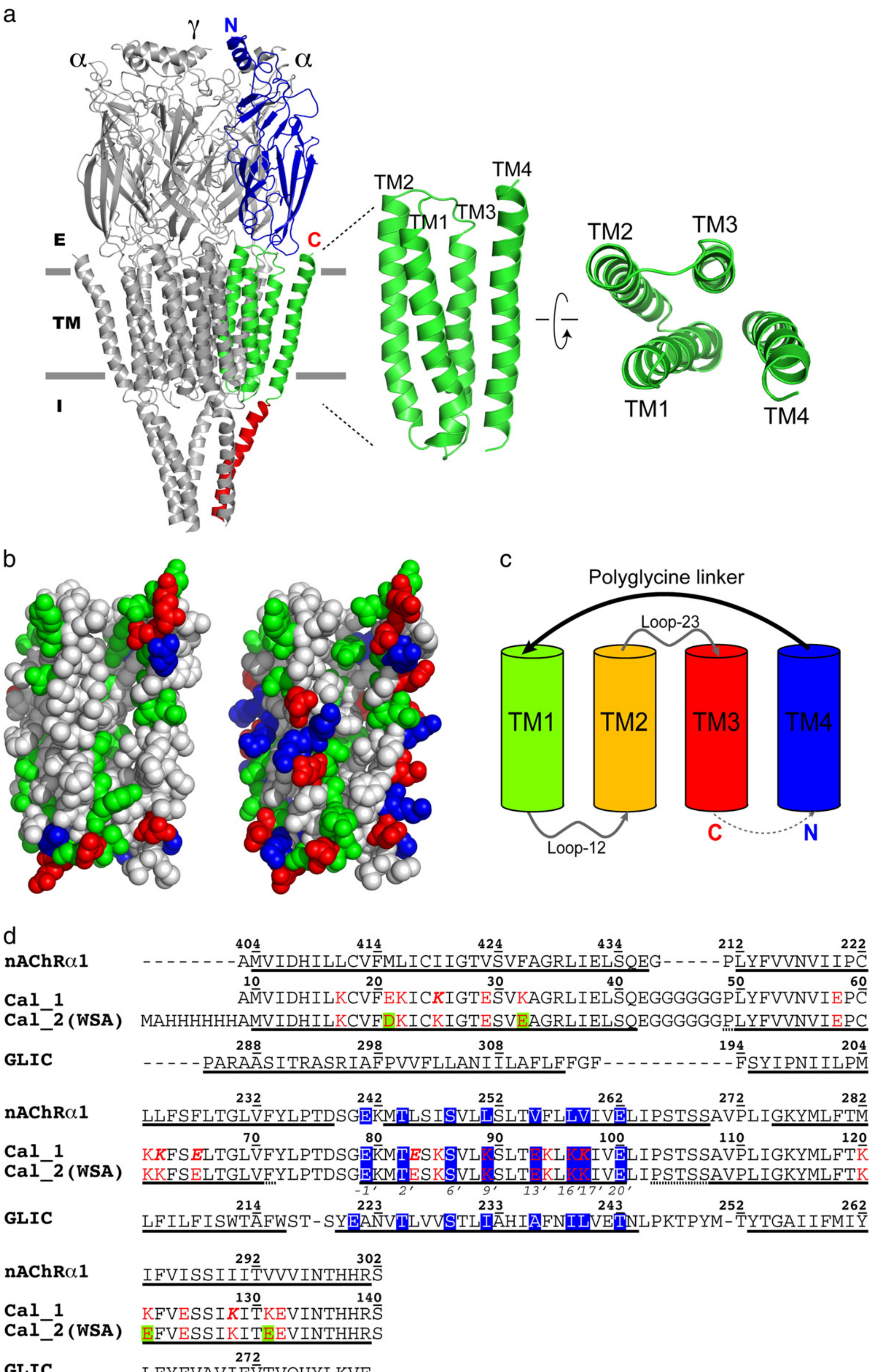
a
α
γ
N
α
E
TM
I
C
TM2
TM4
TM1
TM3
TM2
TM3
TM1
TM4
b
c
Polyglycine linker
Loop-23
TM1
TM2
TM3
TM4
Loop-12
C
N
d
404 414 424 434 212 222
nAChRα1 --------AMVIDHILLCVFMLICIIGTVSVFAGRLIELSQEG-----PLYFVVNVIIPC
10 20 30 40 50 60
Cal_1 AMVIDHILKCVFEKICKIGTESVKAGRLIELSQEGGGGGGPLYFVVNVIEPC
Cal_2(WSA) MAHHHHHHAMVIDHILKCVFDKICKIGTESVEAGRLIELSQEGGGGGGPLYFVVNVIEPC
288 298 308 194 204
GLIC -----PARAASITRASRIAFPVVFLLANIILAFLFFGF-----------FSYIPNIILPM
232 242 252 262 272 282
nAChRα1 LLFSFLTGLVFYLPTDSGEKMTLSISVLLSLTVFLLVIVELIPSTSSAVPLIGKYMLFTM
70 80 90 100 110 120
Cal_1 KKFSELTGLVFYLPTDSGEKMTESKSVLKSLTEKLKKIVELIPSTSSAVPLIGKYMLFTK
Cal_2(WSA) KKFSELTGLVFYLPTDSGEKMTESKSVLKSLTEKLKKIVELIPSTSSAVPLIGKYMLFTK
-1' 2' 6' 9' 13' 16' 17' 20'
214 223 233 243 252 262
GLIC LFILFISWTAFWST-SYEANVTLVVSTLIAHIAFNILVETNLPKTPYM-TYTGAIIFMIY
292 302
nAChRα1 IFVISSIIITVVVINTHHRS
130 140
Cal_1 KFVESSIKITKEVINTHHRS
Cal_2(WSA) EFVESSIKITEEVINTHHRS
272
GLIC LFYFVAVIEVTVQHYLKVE-

defined as the probability of amino acid α summed over the n targeted positions. The effective number of amino acids that appear at the targeted sites, m_{eff}, can be defined using the calculated amino acid probabilities; m_{eff} is bounded $1 \leq m_{eff} \leq m$ and it represents an average over the ensemble of sequences. For a homopolymer where only one amino acid is used to construct the sequence, $m_{eff} = 1$; if all 20 amino acids appear with equal frequency, $m_{eff} = 20$. Thus m_{eff} may be viewed as the effective number of amino acids used to construct the sequences.

The current design focuses on the TM domain without the extracellular domain and the intracellular loop. The removal of the intracellular loop separates TM4 from TM1–TM3. In order to express the designed protein as a single chain, a polyglycine linker was designed using the loop builder in MODELLER [28]. To minimize any structural biases and effects of an artificial linker on TM3 and TM4, and to take advantage of the additional length from the residues in the wild-type sequence leading to the TM1 helix and ending the TM4 helix (the C-terminus), we placed the artificial polyglycine linker between the C-terminus of helix TM4 and the N-terminus of helix TM1 (Fig. 1c). This arrangement preserves the orientations of individual TM domains without restricting the relative spatial positions of TM3 and TM4, as in the topology of the original cryo-EM template.

2.2. Protein expression and purification

Hexahistidine-tagged WSA was expressed using BL21(DE3) competent *Escherichia coli* cells. Cells were first grown at 37 °C in lysogeny broth (LB) media supplemented with 100 μg/ml ampicillin to an OD_{600} of approximately 0.6. Cells were then spun-down and re-suspended into a quarter of the starting volume in ^{13}C- and ^{15}N-rich M9 media containing 100 μg/ml ampicillin and uniformly ^{13}C-labeled glucose and $^{15}NH_4SO_2$ as the sole sources of carbon and nitrogen, respectively. After an hour of recovery at 30 °C, cells were induced with 1 mM IPTG and grown overnight. Cells were then collected by centrifugation at 4 °C and re-suspended in lysis buffer (50 mM Tris–HCl pH 7.5, 15% glycerol and 1 mM NaN_3). The suspended cells were incubated with lysozyme and DNase for ~1 h at room temperature, followed by sonication. The lysate was centrifuged at 18,000 rpm (~3880 *g*) for 20 min. The inclusion bodies were solubilized in 8 M urea in 20 mM Tris–HCl buffer (pH 8.0). After centrifugation (18,000 rpm for 20 min), the supernatant was incubated with 2 ml Ni-NTA resin (Sigma) for 1 h at room temperature. The resin was then washed with 40 ml of the washing buffer (8 M urea, 20 mM Tris–HCl, pH 8.0) and eluted with 6 ml of 250 mM imidazole, 8 M urea, 20 mM Tris–HCl, at pH 8.0. A size exclusion column was optionally used to improve the sample purity. The final protein yield was approximately 7 mg/l from M9 media.

WSA was then refolded in water at pH 8.0 by removing urea through dialysis. The protein was water soluble at high pHs and could be concentrated to at least 2 mg/ml. To prevent soluble aggregation when the pH was adjusted from 8 to 5.8, which was preferred for NMR measurements of the exchangeable backbone amide protons, 2% of 1-palmitoyl-2-hydroxy-*sn*-glycero-3-[phospho-*rac*-(1-glycerol)] (LPPG) (Avanti Lipids) was added to NMR samples to ensure monodispersity of the solubilized WSA.

2.3. Circular dichroism (CD)

CD measurements were performed using a Jasco Model J-810 spectrophotometer and analyzed using the K2D algorithm on the DICHROWEB server.

2.4. NMR spectroscopy and structure determination

Uniformly ^{15}N- and ^{13}C-labeled WSA was prepared in 2% LPPG, 10% D_2O, and 20 mM sodium phosphate buffer at pH 5.8. NMR data were collected at 40 °C using Bruker Avance 600, 700, 800, or 900 MHz spectrometer controlled by the Topspin 1.3 software. The following pulse sequences from the Topspin sequence library were used for backbone and side chain spectral assignment: HNCOCA, HNCA, HNCACB, CBCACONH, HCCH-TOCSY, and 3D ^{15}N- and ^{13}C-edited NOESY. Mixing times for the 3D NOESY spectra were 120 ms and 150 ms for ^{15}N-edited NOESY, and 150 ms for ^{13}C-edited NOESY. Most of the 3D experiments were acquired with a complex time domain size of 1024 (direct observation dimension) × 48–80 (edit dimension) × 128–256 (indirect observation dimension).

The longitudinal and transverse relaxation rate constants, R_1 and R_2, and the steady-state $^{15}N-\{^1H\}$ NOE were measured at 14.1 T using 4, 2.5, and 4 s recycle delays, respectively. R_1 was recorded with 9 inversion-recovery times: 10, 50, 150, 300, 600, 1000, 1600, 2200, 3000 ms. R_2 was recorded using 7 spin-echo delays: 16, 32, 48, 64, 96, 128, and 176 ms. The steady-state $^{15}N-\{^1H\}$ NOE was measured with and without ^1H saturation in an interleaved fashion. The R_2 dispersion measurements were carried out at 14.1 T and 40 °C using the relaxation-compensated, constant-time, Carr–Purcell–Meiboom–Gill (CPMG) sequence with the following 8 CPMG field strengths: 25, 50, 75, 100, 150, 250, 400, and 650 Hz [29,30]. The reference spectrum was acquired without the CPMG period. A relaxation delay of 2.5 s was used.

The NMRPipe [31] and Topspin programs were used to process the NMR spectra. The Sparky program [32] was used for resonance assignments. Structure calculation was performed using CYANA 2.1 [33] based on the distance constraints generated from ^{15}N- and ^{13}C-edited NOESY data, the dihedral angle constraints predicted by Talos [34] based on the chemical shifts, and the hydrogen bonding restraints derived from the temperature effect on the proton chemical shifts [35]. A total of 100 structures were calculated and the 30 structures with the lowest target function were refined using Cyana 3.0. The top 15 structures were further analyzed using Procheck-NMR [36,37] and rendered using VMD [38] and Pymol [39].

The ^{15}N relaxation parameters and $^{15}N-\{^1H\}$ NOE were analyzed quantitatively using DYNAMICS with the extended model-free approach [40,41]. A $^{15}N-^1H$ internuclear bond distance of 1.02 Å and a ^{15}N chemical shift anisotropy of −170 ppm were used. The global tumbling correlation time (τ_m) was determined by an extensive search for the τ_m value that gives the minimum χ^2 value and the least number of non-fitted residues in the Modelfree data fitting.

2.5. Photoaffinity labeling and anesthetic binding analysis

WSA expressed and purified as above was diluted into phosphate-buffered saline, pH 7, at 1 mg/ml, with either azi-isoflurane (1 mM final) or azi-propofol-m (azi-P*m*, 100 μM final) added. These solutions were exposed to 300 nm or 350 nm light, respectively, at ~1 cm distance for 15 min in 300-μl, 1-mm pathlength quartz cuvettes. Samples were then washed with 3 kDa centrifuge filters, and submitted for nano-LC/MS analysis. Briefly, samples were trypsinized and injected into a 10-cm C18 capillary column run at 200 nl/min for 60 min with gradient elution. MS-detected peptides were searched for adducts of the appropriate mass (196 Da for azi-isoflurane; 217 Da for azi-P*m*) and then further fragment patterns were searched using *Sequest* to determine the adduct attachment site. MS work was performed at the University of Pennsylvania Proteomics Core Facility.

3. Results

3.1. WSA sequence design

Using the cryo-EM structure model of the nAChR α1 subunit [3,4] as a template and 40% solvent accessibility surface as the criterion for exposed residues, we identified 29 hydrophobic residues within the TM domains as potential redesign targets. Of these, six residues at the interfaces between the helices were considered and kept unchanged: I219, M243, V261, F414, I420 and V425. The remaining

23 positions were targeted for computational redesign. They are I220, L223, L224, F227, L245, I247, L251, V255, F256, L258, V259, M282, I283, I286, I290, V293, V294, L411, M415, L416, I419, V423, and F426.

At the first stage of site-specific probability computation, the most probable amino acids at each of the 23 positions were calculated. The resulting sequence is shown in Fig. 1d as Cal_1. This sequence was found to be cytotoxic to *Escherichia coli*, and the resulting expression yield was low. In the second stage of redesign, only the positions with amino acid probability >0.8 were constrained to the most probable amino acids. The following six mutations satisfied this condition: L224K, F227E, L245E, V259K, I290K and I419K. At the remaining 17 positions, sequence diversity constraints were used according to Eqs. (1) and (2). With 23 variable residues, the site-specific probabilities yield $m_{eff}=4.3$ in the absence of any constraints on diversity. With the mutations at the above six positions fixed, the constraint was applied so as to achieve $m_{eff}=5.0$. The most probable amino acid was selected at each of the 17 variable positions, yielding sequence Cal_2 in Fig. 1d. This sequence has a theoretical isoelectric point (pI) of=6.39 [42]. Also displayed in Fig. 1d is an aligned sequence for the GLIC TM domains. The sequences are 83% identical between Cal_2 and the original α1 subunit of nAChR, and 11% between Cal_2 and GLIC. The residue numbering used in this study and the corresponding sequence numbering in the nAChR α1 subunit and in GLIC are shown in Fig. 1d.

The lengths of the polyglycine linker (4 to 8 Glys) were investigated, and 50 independent calculations for each length of loop were performed using MODELLER [28]. The 5-glycine segment had the lowest effective energy (best score in MODELLER). The quality of the choice of loop length was also confirmed by energy minimization of the loop structures with NAMD [43] using the CHARMM force field [44].

3.2. Secondary structure of WSA by CD and NMR

CD measurements of WSA in water with 2% LPPG show an α-helical content of ~50% (Fig. 2a), significantly lower than the helical content of the cryo-EM template (~83–87%) used in the sequence redesign, but in reasonable agreement with the estimation from FTIR and CD measurements of the authentic full-length nAChR [45] and GlyR [46,47]. NMR chemical shift index (CSI), which provides residue-specific measures of the secondary structure, clearly shows four helical segments in WSA (Fig. 2b), with ~70% residues having a C_α chemical shift consistent with an α-helix secondary structure. This result is in excellent agreement with the helical content of the TM domains of GLIC. It is worth noting that residues S104-T105-S106-S107 (S266–S269 in the original sequence) between the TM2 and TM3 domains showed two sets of peaks (Fig. 2c and Supplemental Fig. S1): one has α-helical CSI, whereas the other set is non-helical. The fact that two peaks were observed on the NMR timescale for each residue indicated co-existence of two conformations in slow conformational exchange in this segment.

3.3. High-resolution NMR structure of WSA

The advantage of water solubilization of TM channel proteins is clearly displayed in the NMR spectra of WSA (Fig. 3a). Not only can WSA be expressed and purified in a large quantity for structural studies, the NMR spectra also showed that the water solubilization of this TM protein greatly improved monodispersity of the protein sample, allowing high-resolution NMR spectra to be acquired with homogenous peak intensities. Well-resolved 3D NMR spectra permitted spectral assignment of nearly all backbone resonances and many side chain resonances. With the exception of the segment STSS mentioned above, the majority of residues in the WSA sequence showed one set of NMR peaks, indicating a structural homogeneity. A total of 1165 NOE cross peaks were assigned, of which 42 were long-range inter-helical NOEs. These inter-helical NOEs defined the tertiary fold of WSA. The structures of WSA with the STSS segment in the major and minor conformations

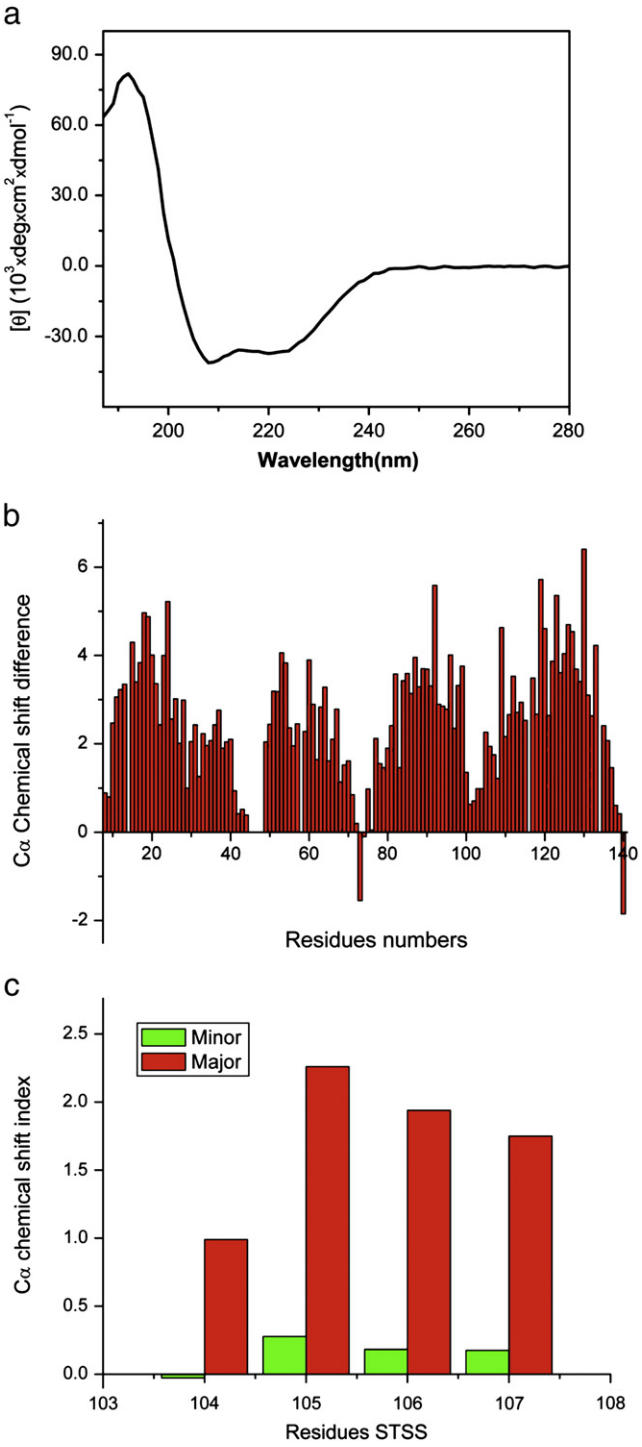

Fig. 2. Secondary structure determination. (a) Far-UV circular dichroism (CD) spectrum of WSA in water with 2% LPPG, showing an α-helical content of ~50%. (b) The NMR chemical shift index (CSI), determined based on the backbone C_α resonance frequencies relative to the random coil values, is plotted as a function of residue numbers. Four helical domains are clearly defined. (c) Conformation heterogeneity in the segment between TM2 and TM3 is visible in the resonance peak doubling for residues S104-T105-S106-S107. SCI suggests slow exchange between helical and non-helical conformations.

were determined separately using standard solution-state NMR methods. The 15 lowest target-function structures for each conformation are shown in Fig. 3b (PDB ID: 2LKG and PDB ID: 2LKH for the major and minor conformations, respectively), and the structure with minimal root-mean-square deviation (RMSD) from the rest in the same conformation is highlighted in the ribbon representation. The

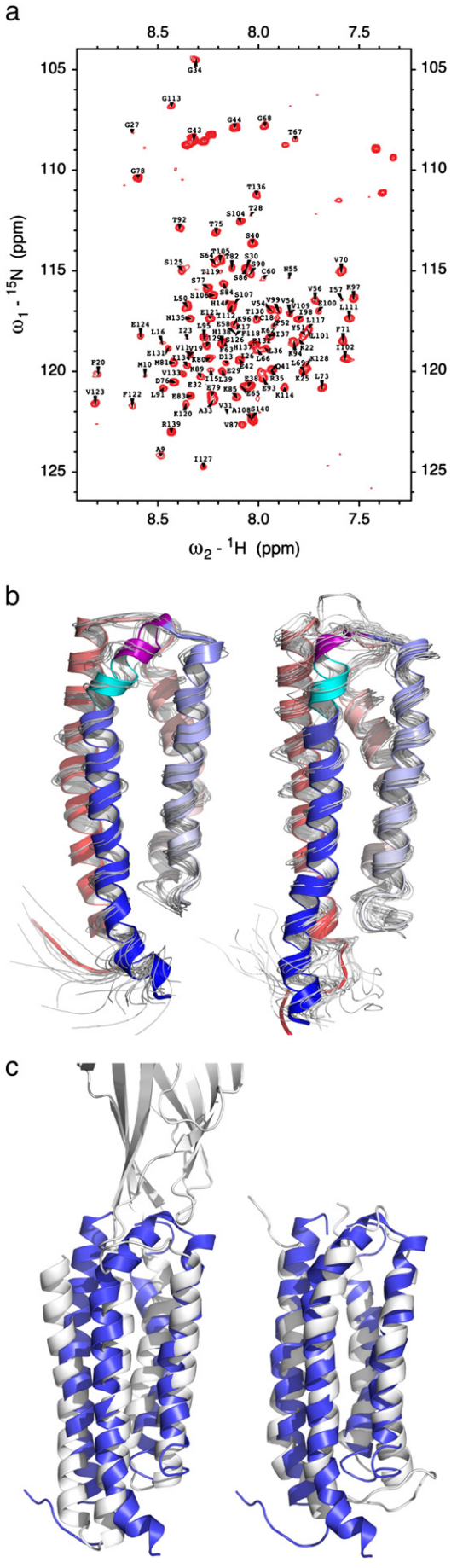

Table 1
Statistics of the NMR structures of WSA in major conformation.

NMR structure	Statistics
Number of distance restraints	1165
Intraresidue ($\|i-j\|=0$)	426
Short range ($\|i-j\|=1$)	423
Medium range ($1<\|i-j\|\leq 4$)	274
Long-range, inter-helical ($\|i-j\|\geq 5$)	42
Number of dihedral angle restraints	211
Number of hydrogen bond restraints	64
Number of upper limit restraints violations >0.5 Å	0
Number of dihedral angle restraints violations >5°	0
Backbone RMSD (Residues 11–40, 50–69, 80–95, 110–132)	0.69 ± 0.13 Å
Heavy atom RMSD (Residues 11–40, 50–69, 80–95, 110–130)	1.06 ± 0.12 Å
Ramachandran plot	
Residues in most favored regions	93.2%
Residues in additionally allowed regions	6.0%
Residues in generously allowed regions	0.9%
Residues in disallowed regions	0.0%

NOE connectivity and hydrogen bonding constraints are depicted in Supplemental Fig. S2. The statistics of the structure calculation and results of the structure analyses are given in Tables 1 and 2 for the major and minor conformations, respectively. The backbone RMSD over the four helical domains is 0.69 ± 0.13 Å and 0.93 ± 0.19 Å for the major and minor conformations, respectively. None of the structures have a distance violation >0.5 Å or an angle violation >5°, and 99.2% of the residues are in the most favored and additional allowed regions of the Ramachandran plot and no residues are in the disallowed region.

3.4. Backbone dynamics of WSA

Backbone ^{15}N R_1 and R_2 relaxation parameters, as well as the steady-state heteronuclear NOEs, were measured for WSA at 14.1 T (600 MHz for ^1H resonances). R_2/R_1 ratios were calculated for all residues. Fig. 4a summarizes these backbone dynamics data. The majority of the R_1 values are between 0.8 and 1.2 s^{-1}, and the R_2 values range from 7 to 18 s^{-1}. The hetNOE values are >0.6 for most of the residues in the helical regions, but significantly lower in the poly-glycine linker and loops between TM1 and TM2 (Loop-12) and between TM2 and TM3 (Loop-23). The average R_2/R_1 ratio for WSA is ~15, suggesting that the NMR data describes a monomeric form of WSA as designed.

Quantitative analyses with the extended model-free approach were performed using the program DYNAMICS [41]. The overall correlation time used in the calculation was 12 ns, which was determined by minimizing the reduced χ^2 value. Results are also depicted in Fig. 4b. The analyses yielded the generalized order parameters (S^2), the local correlation times (τ_e), the exchange term (R_{ex}), the generalized order parameter for the fast effective local motion (S_f^2), and the models used to fit the data for each residue. S^2 is above 0.7 and S_f^2 is 1 in the helical regions, which are typical for globular proteins. For the loop regions, most residues have τ_e ~1–3 ns and S_f^2 is smaller than 1. Several residues displayed non-zero R_{ex} contributions to R_2, indicating that these residues might undergo conformation exchange. Particularly, the TM2 region showed more non-zero R_{ex} terms

Fig. 3. Structure determination of WSA by high-resolution NMR. (a) Representative $^1H-^{15}N$ HSQC NMR spectrum of WSA acquired at 40 °C on an 800-MHz spectrometer, showing well resolved resonances of the water-solubilized membrane protein. (b) Bundles of the 15 lowest target function structures of major (left) and minor (right) conformations. The structures with the least RMSD from the rest of the bundle are depicted in the ribbon representation, with the TM4–TM1–TM2–TM3 domains colored in a red-to-blue color scale. The STSS segment is highlighted in magenta, and Loop-23 in the Cryo-EM template, which is a part of the TM3 helix in the WSA structure, is highlighted in cyan. (c) Superposition of the WSA NMR structure (blue) onto the TM domains of the crystal structure of GLIC (left, white) and the NMR structure of nAChR β2 subunit (right, white), which was solved in hexafluoroisopropanol [6].

Table 2
Statistics of the NMR structures of WSA in minor conformation.

NMR structure	Statistics
Number of distance restraints	1143
Intraresidue ($\|i-j\|=0$)	414
Short range ($\|i-j\|=1$)	416
Medium range ($1<\|i-j\|\leq 4$)	271
Long-range, inter-helical ($\|i-j\|\geq 5$)	42
Number of dihedral angle restraints	201
Number of hydrogen bond restraints	64
Number of upper limit restraints violations > 0.5 Å	0
Number of dihedral angle restraints violations > 5°	0
Backbone RMSD (Residues 11–40, 50–69, 80–95, 110–132)	0.93 ± 0.19 Å
Heavy atom RMSD (Residues 11–40, 50–69, 80–95, 110–132)	1.28 ± 0.18 Å
Ramachandran plot	
Residues in most favored regions	92.0%
Residues in additionally allowed regions	7.2%
Residues in generously allowed regions	0.8%
Residues in disallowed regions	0.0%

than other TM domains. This likely resulted from the computational redesign to promote monomeric structure, where the restriction from other TM2 domains that would otherwise be present in a pentameric structure is removed. CPMG R_2 dispersion measurements, which can detect slow motion on the μs-ms timescale, confirmed the presence of conformational exchanges in the TM2 domain and in Loop-12 and Loop-23 (Fig. 4c). In particular, residues T105 and S106, which are a part of the STSS segment and show two sets of NMR peaks, have non-zero R_{ex}. The adjacent segment V109-P110-L111-I112 (271VPLI274), which forms Loop-23 in the *Torpedo* cryo-EM structure, also shows R_2 dispersion (V109) and non-zero R_{ex} (L111), suggesting conformational flexibility in this region.

3.5. Anesthetic binding to WSA

Using photoaffinity labeling, we investigated potential anesthetic binding to WSA. Peptides accounting for 48% of the sequence were detected for the azi-isoflurane labeled sample, and a single adduction site was found at V-31. Similarly, peptides accounting for 67% of the WSA sequence were detected in the aziP*m* labeled sample, and the same residue (V-31) was found to be the only modified site.

4. Discussion

4.1. Structural characteristics of WSA

We have solved the structure of a water-solubilized analog of the TM domains of the nAChR α1 subunit using solution-state NMR spectroscopy. The protein was designed to be monomeric in solution, permitting secondary and tertiary structures to be determined at atomic resolution. For clarity, we focus our discussion on the WSA structures with the STSS segment in its major conformation. The structure shows the expected four-helix bundle fold, but with four unequal helix lengths. TM1 and TM2 are both six helix-turns long, shorter than TM3 (9 helix turns) and TM4 (8 helix turns). In comparison, the cryo-EM structure of *Torpedo* nAChR, which was used as the template in the computational sequence redesign, has four straight helices of roughly equal lengths (8 helix turns for TM1, TM2, and TM3, and 10 helix turns for TM4). The residues belonging to the helices as determined in the cryo-EM structure and the WSA NMR structure, along with those in the crystal structure of GLIC, are underlined in the sequences in Fig. 1 for comparison. A superposition of WSA structure onto the monomer structure of GLIC is depicted in Fig. 3c.

Although WSA has ~83% sequence identity to the wild-type nAChR and only 11% identity to the GLIC TM domains, the high-resolution NMR structure of WSA agrees more with that of GLIC than with the cryo-EM template. This is rather unexpected. Several

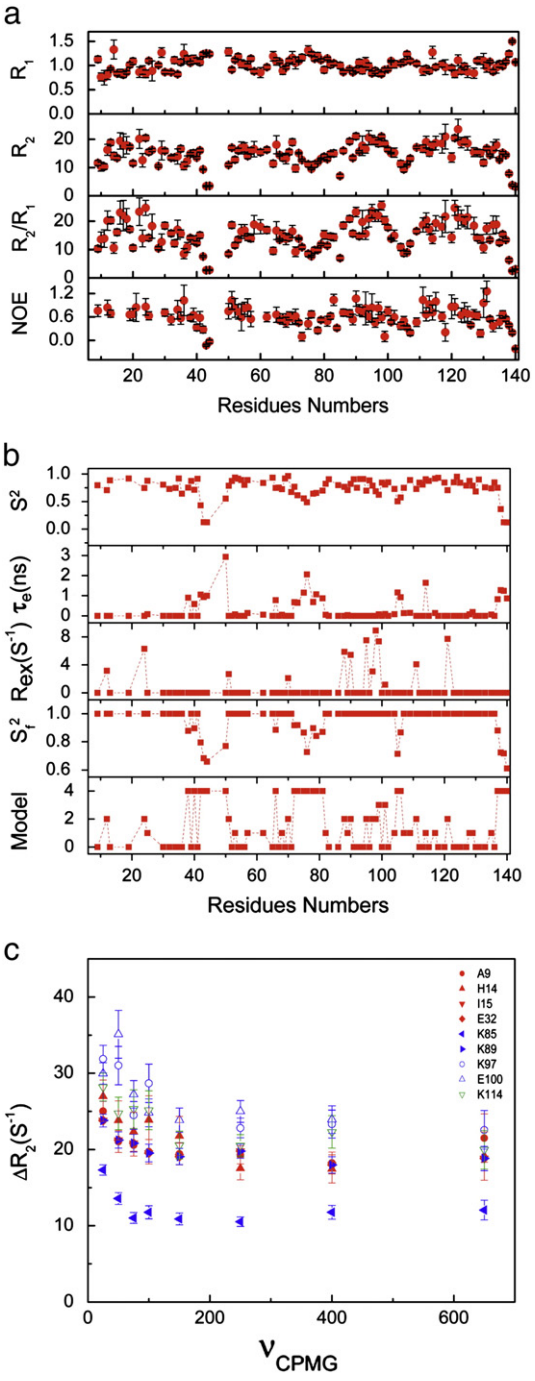

Fig. 4. Dynamics analysis of WSA. (a) Backbone amide ^{15}N relaxation of WSA was measured at pH 5.5 and 40 °C using a 600-MHz spectrometer. Longitudinal and transverse relaxation rate constants, R_1 and R_2, respectively, and $^{15}N-^{1}H$ steady-state nuclear Overhauser effect (NOE) are plotted as a function of residue numbers. Error bars are the standard errors of fitting to the exponential decay function for R_1 and R_2 and the calculated uncertainties for NOE. (b) Quantitative model-free analysis of WSA dynamics using DYNAMICS program. S^2, generalized order parameters; τ_e, the correlation time of local motion; R_{ex}, exchange contribution to R_2 relaxation; S_f^2, generalized order parameters for effective fast local motion. (c) Representative R_2 dispersions are plotted as a function of ν_{CPMG} in unit of Hz, showing dynamics on the μs-ms timescale (TM2, blue; TM3, green; and TM4, red).

contributing factors can be considered. First, the experimental conditions under which the structures were determined were very different. The cryo-EM structure of nAChR was determined in highly ordered tubular crystal arrays rapidly frozen in liquid–nitrogen-cooled ethane. WSA NMR structure was determined at room

temperature in a significantly more dynamic aqueous solution of lyso-lipids; 2% LPPG was needed to maintain monodispersity of the NMR sample when pH was lowered to 5.8. Similarly, GLIC was crystallized at a non-freezing temperature in ~3% *n*-Undecyl-β-D-maltoside detergent. Moreover, nAChR normally resides in eukaryotic membranes that contain cholesterol, and cholesterol has been proposed to form a slowly exchangeable structural component of this family of ligand-gated ion channels [48]. The absence of cholesterol in WSA may therefore make it more analogous to the GLIC structure. Hence, the environment might play a more critical role than the amino acid sequences in affecting the high-resolution details of the structures. The debatable question remains as to which biophysical conditions are more relevant for membrane protein structure determination. Before high-resolution structures can be determined under physiologically relevant conditions, all currently available methods, including crystallography, can conceivably introduce some degree of artifact. Second, the high-resolution difference between WSA and cryo-EM nAChR structures may result from different equilibriums of conformational states. The cryo-EM structure is believed to mainly capture the closed state of the channel [3], whereas GLIC crystal is thought to be in either an open or desensitized state [9,10]. Because the WSA structure was determined as a monomer, its conformational state can only be inferred. The fact that the WSA structure agrees so well with the GLIC structure suggests that the WSA monomer may reflect the conformation of the open or desensitized state of the nAChR TM domains. Third, there is also a possibility that the WSA structure is distorted due to the absence of extracellular and intracellular domains or due to water solubilization itself. This scenario is very unlikely, however, given the agreement between WSA and GLIC structures. GLIC was determined as an intact channel protein. Taken together, our results suggest that water-solubilization of membrane proteins is equally relevant for structure determination compared to more conventional lipid or detergent solubilization approaches. The ease in protein expression and purification and, more importantly, the greatly improved spectral quality of the resulting proteins after water solubilization, make water solubilization an attractive alternative. We believe that the NMR structures of water-solubilized proteins, including WSK3 published previously [13] and WSA determined in this study, represent the first approximation of the native structures. These structures provide the high-resolution templates for further refinement by other biophysical means.

4.2. Dynamic characteristics of WSA

It is conceivable that water solubilization of membrane proteins can change the motional characteristics of these proteins. For WSA, several residues in the TM2 domain were mutated from hydrophobic to charged amino acids for the purpose of promoting monomeric form in order to increase NMR spectral resolution. There are seven mutations in the TM2 helix, four of which, L89K (L9′K), V93E (V13′E), L96K (L16′K), and V97K (V17′K) (see Fig. 1d for relative numbering of TM2), are located at the putative pore-lining sites of the nAChR channel. The charged residues likely prevent the formation of oligomerization by TM2. Without association with other TM2 helices, the TM2 domain becomes particularly dynamic in WSA. Both backbone dynamics measurements and R_2 dispersion measurements showed either non-zero R_{ex} contributions to the R_2 relaxation (residues 8′, 10′, 15′, 17′, 18′, and 19′, see Fig. 4) or R_2 dispersion on the μs timescale (residues −2′, 2′, 5′, 9′, 17′, and 20′). The slow motion captured in R_2 dispersion suggests possible conformation exchange. In comparison, TM1, TM3, and TM4 domains showed significantly fewer numbers of residues with R_{ex} term and R_2 dispersion (Fig. 4). Although the increase in dynamics of TM2 in WSA is undoubtedly the result of water solubilization, the fact that other TM domains do not experience the same degree of increase suggests that the motional characteristics of TM2, controlled by Loop-12 and Loop-23, might be intrinsically different from the rest of the protein. Indeed, it has been suggested that nAChR TM domains can be separated into inner helices, comprised of TM2 domains, and outer helices, comprised of TM1, TM3, and TM4 helices [3]. Channel gating is thought to involve the movement of the inner helices relative to the outer helices.

The dynamics of the two loops, Loop-12 and Loop-23, deserves further examination. As shown in Fig. 1d, the WSA loop regions coincide more with those in the GLIC structure than in the nAChR cryo-EM structure. Loop-12 consists of five residues L73-S77 (LPTDS) in WSA, which differs from the very tight, three-residue turn (SGE) in the cryo-EM structure. The loop residues are also shifted. Loop-12 in WSA is a part of the TM1 helix in the nAChR cryo-EM structure, whereas Loop-12 in the cryo-EM structure forms the beginning of the TM2 helix in WSA. The NMR dynamics measurements show that the segment from Y72 to K80, encompassing Loop-12 in both the WSA (LPTDS) and cryo-EM (SGE) structures, is highly flexible. The relaxation data in this segment can only be fitted with model 4 or model 5 with ~1–3 ns local motions (τ_e) and reduced S^2 and S_f^2 (see Fig. 4b). Although the Loop-12 conformation as shown in the NMR structures is the preferred conformation based on the NMR data, the shifted Loop-12 conformation as displayed in the Cryo-EM structure is also possible. We found that E79 (E–1′) did not meet the basic Lipari–Szabo assumption in the model-free analysis and could only be fitted by model 5. The adjacent residue, G78 (G–2′), shows R_2 dispersion on the μs timescale. Nevertheless, we believe that the Loop-12 conformation as shown in the NMR structures, with P74 in the loop instead of in the TM1 helix, is the dominant loop population in the conformational equilibrium.

Similarly, Loop-23 between the TM2 and TM3 domain is also highly dynamic. In the intact receptor, this loop is believed to interact with the Cys-loop and β12 loop in the extracellular domain to mediate ligand binding to channel gating [17,18,49,50]. In the WSA structure, the TM2 helix ends at E20′, whereas in the Cryo-EM structure, the TM2 helix extends to the extracellular space and ends at S27′ or A28′. None of the high-resolution structures solved so far for Cys-loop receptors, including the WSA structure solved in this study, the NMR structure of the nAChR β2 subunit TM domains [6], the high resolution NMR structures of glycine receptor TM2–TM3 domains solved in DMPC/DHPC bicelles [51], the crystal structure of GLIC [10], and the crystal structure ELIC [8], agree with the cryo-EM structure in this region. Our dynamics data suggest that several conformations can co-exist in Loop-23. Even with water solubilization, the dynamic characteristics seem to have been preserved. High-resolution NMR spectra of pentameric glycine receptor TM domains in lyso-lipid micelles also exhibit peak doubling in this segment (data not shown), suggesting that slow conformational exchange is an intrinsic dynamic feature in the region between TM2 and TM3 helices. The conformation heterogeneity of Loop-23 may be required for the TM2 movement during channel gating.

4.3. Anesthetic binding to WSA

To further confirm the similarity of WSA to GLIC, we performed binding studies. Recently, X-ray structures of GLIC were solved with two different general anesthetics – propofol and a haloether, desflurane – bound [52]. Like GLIC, nAChR is also sensitive to general anesthetics, so confirmation of anesthetic binding will provide a functional measure of the fidelity of the water solubilization paradigm. We found that both a propofol photolabel and a haloether photolabel bound to the same residue (V31) in the WSA structure (Fig. 5). Also highlighted in this figure are residues that border the propofol-binding site in the GLIC-anesthetic co-crystal structure. The agreement with respect to the Z-direction along the bundle is remarkable. Although the side chain of V31 is oriented away from the intrasubunit GLIC anesthetic site, we have prior evidence suggesting that backbone carbonyl atoms are the preferred photoadduction sites [53], especially for residues with apolar

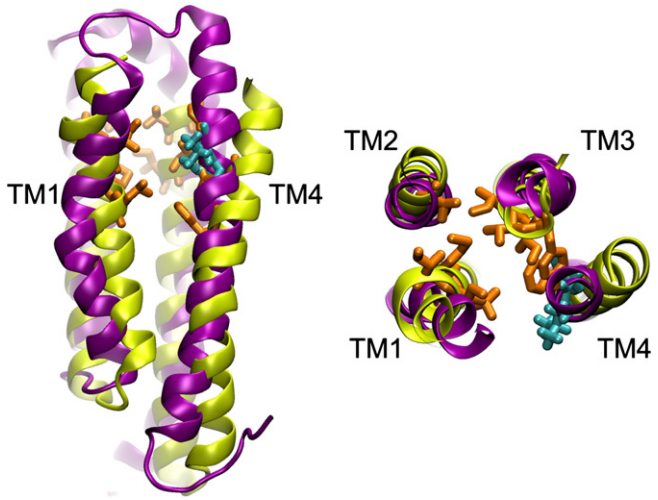

Fig. 5. Comparison of anesthetic binding site in WSA and in GLIC. The WSA structure (purple) is fitted to the TM domain of the crystal structure of GLIC (yellow). The anesthetic binding site in WSA was determined by photoaffinity labeling. Both azi-isoflurane and azi-propofol bind to residue V31 located in TM4 (cyan). The dominant propofol binding site in GLIC crystal is highlighted in orange. Notice that the general location of the binding sites is essentially the same, suggesting that the drug-binding site is preserved in the water-solubilized protein.

hydrocarbon side chains. The V31 carbonyl oxygen is oriented such that it is easily accessed from the intrasubunit cavity. Thus, it would appear that the anesthetic site in GLIC and WSA is similarly positioned within the bundle. This result further validates the water-solubilization approach: mutation of surface residues to improve water solubility does not greatly alter the overall fold and internal packing of the protein, preserving potential drug binding sites for structure-based drug screening. However, it is important to note that neither the propofol nor the isoflurane binding site has been definitely located in nAChR, thus we cannot yet conclude with confidence that the WSA site well represents the anesthetic binding site in the native nAChR.

4.4. WSA-detergent interaction site

Although WSA was soluble in water at a high pH, lowering the pH to pass the theoretical pI for NMR experiments can lead to soluble aggregations. To maintain WSA monodispersity in the NMR sample, 2% of the lyso-lipid LPPG was used. Previous experimental and computational studies have suggested that the nicotinic acetylcholine receptor requires the proper compositions of lipids in order to function. The location of lyso-lipid molecules in WSA can thus provide structural information about protein-lipid interaction. In the ^{15}N-edited NOESY spectra, we found several inter-molecular cross peaks between WSA and LPPG. Absence of cross-peaks does not indicate absence of interactions, but presence of intermolecular NOESY peaks signifies strong and stable interactions. We found that several residues at the TM1 and TM4 interface have cross peaks with LPPG. Specifically, residues 48, 50, 64, and 67 of TM1 and residues 24, 33, 34, 35, 39, 40, 41, and 43 of TM4 border an interfacial cavity that can accept a lipid molecule. The same cavity can be found in the nAChR cryo-EM structure and in ELIC and GLIC X-ray structures. As shown in Fig. S3 in the supplement, the superposition of WSA and GLIC reveals that the strong WSA-LPPG interaction site coincides nearly perfectly with the location where surface lipid molecules were found in the GLIC crystal. This finding indicates that despite water solubilization, the helix interfaces are preserved to maintain possible interactions as in the wild-type protein.

In summary, the monomer structure of a water-soluble analog of the *Torpedo* nAChR α1 subunit was resolved to the backbone RMSD of 0.69 ± 0.13 Å. The overall structure is similar to the crystal structure of GLIC, demonstrating the robustness of the water solubilization approach. The WSA structure preserved the anticipated intra-helical drug binding site and lipid interaction site in the intact form of homologous receptors.

Acknowledgements

This work was supported in part by grants from the National Institutes of Health of the United States (R01GM056257, R37GM049202, and P01GM055876) and the National Science Foundation (NSEC DMR08-32802).

Appendix A. Supplementary data

Supplementary data to this article can be found online at doi:10.1016/j.bbamem.2011.11.021.

References

[1] J.M. Lindstrom, Nicotinic acetylcholine receptors of muscles and nerves: comparison of their structures, functional roles, and vulnerability to pathology, Ann. N. Y. Acad. Sci. 998 (2003) 41–52.
[2] J.E. Baenziger, P.J. Corringer, 3D structure and allosteric modulation of the transmembrane domain of pentameric ligand-gated ion channels, Neuropharmacology 60 (2010) 116–125.
[3] A. Miyazawa, Y. Fujiyoshi, N. Unwin, Structure and gating mechanism of the acetylcholine receptor pore, Nature 423 (2003) 949–955.
[4] N. Unwin, Refined structure of the nicotinic acetylcholine receptor at 4A resolution, J. Mol. Biol. 346 (2005) 967–989.
[5] C.D. Dellisanti, Y. Yao, J.C. Stroud, Z.Z. Wang, L. Chen, Crystal structure of the extracellular domain of nAChR alpha1 bound to alpha-bungarotoxin at 1.94 A resolution, Nat. Neurosci. 10 (2007) 953–962.
[6] V. Bondarenko, T. Tillman, Y. Xu, P. Tang, NMR structure of the transmembrane domain of the n-acetylcholine receptor beta2 subunit, Biochim. Biophys. Acta 1798 (2010) 1608–1614.
[7] K. Brejc, W.J. van Dijk, R.V. Klaassen, M. Schuurmans, J. van Der Oost, A.B. Smit, T.K. Sixma, Crystal structure of an ACh-binding protein reveals the ligand-binding domain of nicotinic receptors, Nature 411 (2001) 269–276.
[8] R.J. Hilf, R. Dutzler, X-ray structure of a prokaryotic pentameric ligand-gated ion channel, Nature 452 (2008) 375–379.
[9] N. Bocquet, H. Nury, M. Baaden, C. Le Poupon, J.P. Changeux, M. Delarue, P.J. Corringer, X-ray structure of a pentameric ligand-gated ion channel in an apparently open conformation, Nature 457 (2009) 111–114.
[10] R.J. Hilf, R. Dutzler, Structure of a potentially open state of a proton-activated pentameric ligand-gated ion channel, Nature 457 (2009) 115–118.
[11] A.M. Slovic, H. Kono, J.D. Lear, J.G. Saven, W.F. DeGrado, Computational design of water-soluble analogues of the potassium channel KcsA, Proc. Natl. Acad. Sci. U.S.A. 101 (2004) 1828–1833.
[12] J. Bronson, O.S. Lee, J.G. Saven, Molecular dynamics simulation of WSK-3, a computationally designed, water-soluble variant of the integral membrane protein KcsA, Biophys. J. 90 (2006) 1156–1163.
[13] D. Ma, T.S. Tillman, P. Tang, E. Meirovitch, R. Eckenhoff, A. Carnini, Y. Xu, NMR studies of a channel protein without membranes: structure and dynamics of water-solubilized KcsA, Proc. Natl. Acad. Sci. U.S.A. 105 (2008) 16537–16542.
[14] Y. Zhou, J.H. Morais-Cabral, A. Kaufman, R. MacKinnon, Chemistry of ion coordination and hydration revealed by a K+ channel-Fab complex at 2.0 A resolution, Nature 414 (2001) 43–48.
[15] T. Cui, C.G. Canlas, Y. Xu, P. Tang, Anesthetic effects on the structure and dynamics of the second transmembrane domains of nAChR alpha4beta2, Biochim. Biophys. Acta 1798 (2009) 161–166.
[16] Y. Xu, T. Seto, P. Tang, L. Firestone, NMR study of volatile anesthetic binding to nicotinic acetylcholine receptors, Biophys. J. 78 (2000) 746–751.
[17] L.T. Liu, E.J. Haddadian, D. Willenbring, Y. Xu, P. Tang, Higher susceptibility to halothane modulation in open- than in closed-channel alpha4beta2 nAChR revealed by molecular dynamics simulations, J. Phys. Chem. B 114 (2009) 626–632.
[18] L.T. Liu, D. Willenbring, Y. Xu, P. Tang, General anesthetic binding to neuronal alpha4beta2 nicotinic acetylcholine receptor and its effects on global dynamics, J. Phys. Chem. B 113 (2009) 12581–12589.
[19] D.C. Chiara, L.J. Dangott, R.G. Eckenhoff, J.B. Cohen, Identification of nicotinic acetylcholine receptor amino acids photolabeled by the volatile anesthetic halothane, Biochemistry 42 (2003) 13457–13467.
[20] R. Fraczkiewicz, W. Braun, Exact and efficient analytical calculation of the accessible surface areas and their gradients for macromolecules, J. Comput. Chem. 19 (1998) 15.
[21] H. Kono, J.G. Saven, Statistical theory for protein combinatorial libraries. Packing interactions, backbone flexibility, and the sequence variability of a main-chain structure, J. Mol. Biol. 306 (2001) 607–628.
[22] J.R. Calhoun, H. Kono, S. Lahr, W. Wang, W.F. DeGrado, J.G. Saven, Computational design and characterization of a monomeric helical dinuclear metalloprotein, J. Mol. Biol. 334 (2003) 1101–1115.
[23] F.V. Cochran, S.P. Wu, W. Wang, V. Nanda, J.G. Saven, M.J. Therien, W.F. DeGrado, Computational de novo design and characterization of a four-helix bundle

protein that selectively binds a nonbiological cofactor, J. Am. Chem. Soc. 127 (2005) 1346–1347.
[24] V. Nanda, M.M. Rosenblatt, A. Osyczka, H. Kono, Z. Getahun, P.L. Dutton, J.G. Saven, W.F. Degrado, De novo design of a redox-active minimal rubredoxin mimic, J. Am. Chem. Soc. 127 (2005) 5804–5805.
[25] G.M. Bender, A. Lehmann, H. Zou, H. Cheng, H.C. Fry, D. Engel, M.J. Therien, J.K. Blasie, H. Roder, J.G. Saven, W.F. DeGrado, De novo design of a single-chain diphenylporphyrin metalloprotein, J. Am. Chem. Soc. 129 (2007) 10732–10740.
[26] R.L. Dunbrack Jr., F.E. Cohen, Bayesian statistical analysis of protein side-chain rotamer preferences, Protein Sci. 6 (1997) 1661–1681.
[27] S.J. Weiner, P.A. Kollman, D.A. Case, U.C. Singh, C. Ghio, G. Alagona, S. Profeta, P. Weiner, A new force-field for molecular mechanical simulation of nucleic-acids and proteins, J. Am. Chem. Soc. 106 (1984) 20.
[28] A. Fiser, R.K. Do, A. Sali, Modeling of loops in protein structures, Protein Sci. 9 (2000) 1753–1773.
[29] J.P. Loria, M. Rance, A.G. Palmer 3rd, A relaxation-compensated Carr–Purcell–Meiboom–Gill sequence for characterizing chemical exchange by NMR spectroscopy, J. Am. Chem. Soc. 121 (1999) 1.
[30] M. Tollinger, N.R. Skrynnikov, F.A. Mulder, J.D. Forman-Kay, L.E. Kay, Slow dynamics in folded and unfolded states of an SH3 domain, J. Am. Chem. Soc. 123 (2001) 11341–11352.
[31] F. Delaglio, S. Grzesiek, G.W. Vuister, G. Zhu, J. Pfeifer, A. Bax, NMRPipe: a multidimensional spectral processing system based on UNIX pipes, J. Biomol. NMR 6 (1995) 277–293.
[32] T.D. Goddard, D.G. Kneller, Sparky 3, University of California, San Francisco, 2002.
[33] P. Guntert, C. Mumenthaler, K. Wuthrich, Torsion angle dynamics for NMR structure calculation with the new program DYANA, J. Mol. Biol. 273 (1997) 283–298.
[34] G. Cornilescu, F. Delaglio, A. Bax, Protein backbone angle restraints from searching a database for chemical shift and sequence homology, J. Biomol. NMR 13 (1999) 289–302.
[35] N.J. Baxter, M.P. Williamson, Temperature dependence of 1H chemical shifts in proteins, J. Biomol. NMR 9 (1997) 359–369.
[36] J.F. Doreleijers, J.A. Rullmann, R. Kaptein, Quality assessment of NMR structures: a statistical survey, J. Mol. Biol. 281 (1998) 149–164.
[37] R.A. Laskowski, J.A. Rullmannn, M.W. MacArthur, R. Kaptein, J.M. Thornton, AQUA and PROCHECK-NMR: programs for checking the quality of protein structures solved by NMR, J. Biomol. NMR 8 (1996) 477–486.
[38] W. Humphrey, A. Dalke, K. Schulten, VMD: visual molecular dynamics, J. Mol. Graph. 14 (1996) 33–38 (27–38).
[39] W. DeLano, PyMOL molecular graphics systemAvailable at, http://www.pymol.org 2002.
[40] G.M. Clore, A. Szabo, A. Bax, L.E. Kay, P.C. Driscoll, A.M. Gronenborn, Deviations from the simple two-parameter model-free approach to the interpretation of nitrogen-15 nuclear magnetic relaxation of proteins, J. Am. Chem. Soc. 112 (1990) 4989–4991.
[41] D. Fushman, S. Cahill, D. Cowburn, The main-chain dynamics of the dynamin pleckstrin homology (PH) domain in solution: analysis of 15N relaxation with monomer/dimer equilibration, J. Mol. Biol. 266 (1997) 173–194.
[42] B. Bjellqvist, G.J. Hughes, C. Pasquali, N. Paquet, F. Ravier, J.C. Sanchez, S. Frutiger, D. Hochstrasser, The focusing positions of polypeptides in immobilized ph gradients can be predicted from their amino-acid-sequences, Electrophoresis 14 (1993) 1023–1031.
[43] J.C. Phillips, R. Braun, W. Wang, J. Gumbart, E. Tajkhorshid, E. Villa, C. Chipot, R.D. Skeel, L. Kale, K. Schulten, Scalable molecular dynamics with NAMD, J. Comput. Chem. 26 (2005) 1781–1802.
[44] A.D. MacKerell, D. Bashford, M. Bellott, R.L. Dunbrack, J.D. Evanseck, M.J. Field, S. Fischer, J. Gao, H. Guo, S. Ha, D. Joseph-McCarthy, L. Kuchnir, K. Kuczera, F.T.K. Lau, C. Mattos, S. Michnick, T. Ngo, D.T. Nguyen, B. Prodhom, W.E. Reiher, B. Roux, M. Schlenkrich, J.C. Smith, R. Stote, J. Straub, M. Watanabe, J. Wiorkiewicz-Kuczera, D. Yin, M. Karplus, All-atom empirical potential for molecular modeling and dynamics studies of proteins, J. Phys. Chem. B 102 (1998) 31.
[45] U. Gorne-Tschelnokow, A. Strecker, C. Kaduk, D. Naumann, F. Hucho, The transmembrane domains of the nicotinic acetylcholine receptor contain alpha-helical and beta structures, EMBO J. 13 (1994) 338–341.
[46] M. Cascio, S. Shenkel, R.L. Grodzicki, F.J. Sigworth, R.O. Fox, Functional reconstitution and characterization of recombinant human alpha 1-glycine receptors, J. Biol. Chem. 276 (2001) 20981–20988.
[47] D. Ma, Z. Liu, L. Li, P. Tang, Y. Xu, Structure and dynamics of the second and third transmembrane domains of human glycine receptor, Biochemistry 44 (2005) 8790–8800.
[48] G. Brannigan, J. Henin, R. Law, R. Eckenhoff, M.L. Klein, Embedded cholesterol in the nicotinic acetylcholine receptor, Proc. Natl. Acad. Sci. U.S.A. 105 (2008) 14418–14423.
[49] D. Mowrey, E.J. Haddadian, L.T. Liu, D. Willenbring, Y. Xu, P. Tang, Unresponsive correlated motion in alpha7 nAChR to halothane binding explains its functional insensitivity to volatile anesthetics, J. Phys. Chem. B 114 (2010) 7649–7655.
[50] A. Szarecka, Y. Xu, P. Tang, Dynamics of heteropentameric nicotinic acetylcholine receptor: implications of the gating mechanism, Proteins 68 (2007) 948–960.
[51] C.G. Canlas, D. Ma, P. Tang, Y. Xu, Residual dipolar coupling measurements of transmembrane proteins using aligned low-q bicelles and high-resolution magic angle spinning NMR spectroscopy, J. Am. Chem. Soc. 130 (2008) 13294–13300.
[52] H. Nury, C. Van Renterghem, Y. Weng, A. Tran, M. Baaden, V. Dufresne, J.P. Changeux, J.M. Sonner, M. Delarue, P.J. Corringer, X-ray structures of general anaesthetics bound to a pentameric ligand-gated ion channel, Nature 469 (2011) 428–431.
[53] R.G. Eckenhoff, J. Xi, M. Shimaoka, A. Bhattacharji, M. Covarrubias, W.P. Dailey, Azi-isoflurane, a Photolabel Analog of the Commonly Used Inhaled General Anesthetic Isoflurane, ACS Chem. Neurosci. 1 (2010) 139–145.